MODULATING SIZE AND SURFACE CHARGE OF ETHYLCELLULOSE NANOPARTICLES THROUGH THE USE OF CATIONIC NANO-EMULSION TEMPLATES

G. Calderó[1], S.Leitner[1], M.J. García-Celma[2,1] and C. Solans[1]

[1] Institut de Química Avançada de Catalunya (IQAC-CSIC). Jordi Girona 18-26, 08034 Barcelona, Spain. Centro de Investigación Biomédica en Red en Bioingeniería, Biomateriales y Nanomedicina (CIBER-BBN), Barcelona, Spain

[2] Departament de Farmàcia i Tecnologia Farmacèutica i Fisicoquímica. Univ. de Barcelona. Unitat Associada d'I+D al CSIC, IN2UB, Av Joan XXIII, s/n, 08028 Barcelona, Spain

GRAPHICAL ABSTRACT

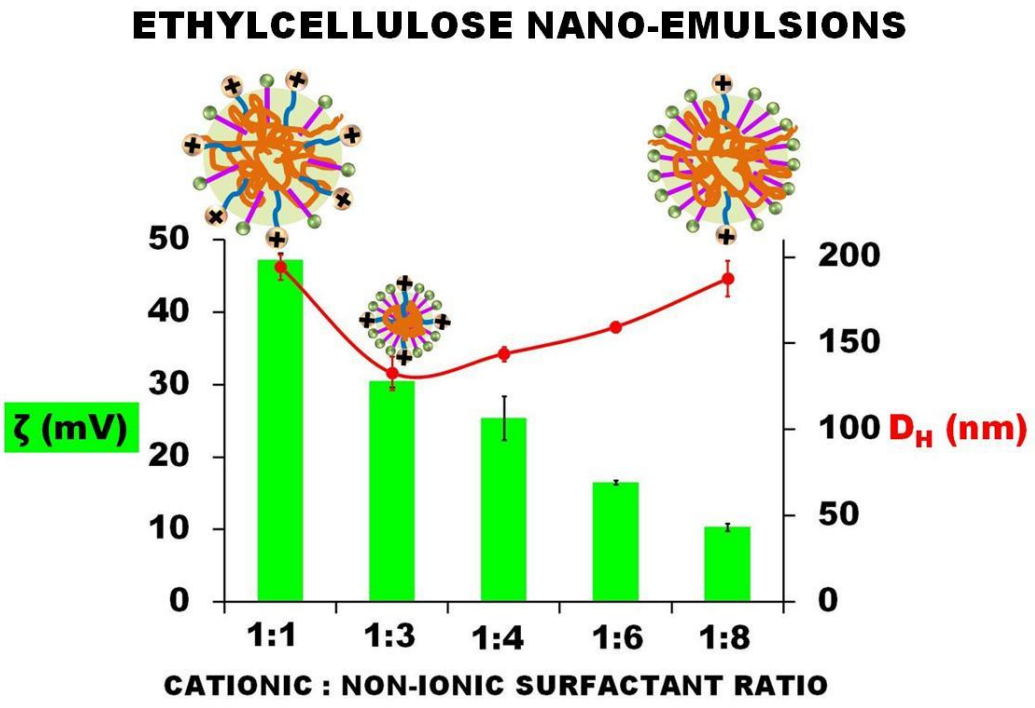

ABSTRACT

Ethylcellulose nano-emulsions have been obtained by the low-energy phase inversion composition method in the Water / [Alkylamidoammonium: Cremophor WO7] / [6% ethylcellulose in ethyl acetate] system at 25ºC. It is shown that nano-emlulsions' composition variables (oil-to-surfactant ratio, cationic: nonionic surfactant ratio and polymer and water content) produce changes in their droplet diameter, surface charge and colloidal stability following defined trends. Nano-emulsions with good stability, droplet diameters between about 120 and 200 nm and surface charge from about 10 to 50 mV have been obtained. Nano-emulsions are further used as templates for nanoparticle dispersions preparation, which show sizes and surface charges typically smaller and similar respectively to their nano-emulsion templates. Cationic: nonionic surfactant ratio has the highest influence on both, size and surface charge, followed by oil-to-surfactant ratio and water content. Interestingly, the positive charge of the nanoparticles can be depleted under diluting conditions in a time-dependent manner.

KEYWORDS

Ethylcellulose; nano-emulsion; PIC method; cationic nanoparticles; alkylamidoammonium; zeta potential

1. INTRODUCTION

Ethylcellulose is a semisynthetic cellulose derivative, insoluble in water, which has attracted increasing attention for its interesting properties, including film, fiber and particle forming ability, mechanical strength, flexibility, thermoplasticity, transparency, lack of taste and odor, etc. (Heseltine et al. 2018; Crabbe-Mann et al. 2018; Davidovich-Pinhas et al. 2014). In addition, ethylcellulose is physiologically inert and biocompatible, and is listed as "GRAS" (*Generally Recognized as Safe*) by the Food and Drug Administration. Numerous uses

have been reported so far for this polymer, encompassing a broad range of fields of application, such as coatings and films for batteries and other engineering components (Cao et al. 2018; Zuo et al 2018), wound-dressing materials (Crabbe-Mann et al. 2018), or food texturizers, edible oleogels and flavor delivery systems (Eltayeb et al. 2015; Davidovich-Pinhas et al. 2015; Gravelle et al. 2018) to mention a few.

Nowadays, a matter of concern is the development of materials and processes which are both, environmental friendly and safe. These issues have progressed in the last decades for example by the replacement of contaminant and toxic solvents by greener and milder ones, or by favouring gentle, energy-saving processes such as those avoiding heating and/or cooling steps or those based in self-assembly (Spernath et al 2007; Calderó et al. 2011; Eltayeb et al. 2015; Crabbe-Mann et al. 2018; Hayden et al. 2018; Leitner et al. 2019). For example, ethylcellulose submicron materials have been prepared using the supercritical antisolvent precipitation method, which is considered a clean technology, although it requires specific equipment (Djerafi et al. 2015). More recently, a new electrodynamic process using environmentally friendly and low toxicity solvent systems has been reported for the preparation of a wide range of ethyl cellulose microstructures encompassing particles and fibres (Crabbe-Mann et al. 2018). Although this method does not require surfactants, materials produced are in the micrometric size range. Achievement of smaller particles in the nanosized range can be attained by other methods, such as low-energy emulsification approaches, with the help of surfactant molecules. Nanosized ethylcellulose particles are attracting increasing interest, as this polymer is biostable and biocompatible. It has been shown to be specially suited for the encapsulation and the controlled release of a large variety of active ingredients, including drugs (Calderó et al. 2016; Hiew et al 2019), biosensors for “in vitro” diagnostics (Generalova et al. 2009), cosmetic agents such as organic UV filters (Hayden et al. 2018), or agrochemical components like insect pest control agents (Elek et al.2010). In the textile field, ethylcellulose nanoparticles have been used to design functional fabrics for the release of active ingredients (Vilchez et al. 2014). Research carried out in the last decade focusing on the preparation of ethylcellulose nanoparticles by a low-energy emulsification

method (the phase-inversion composition, PIC, method) followed by solvent evaporation, has allowed replacing frequently used halogenated aromatic solvents by ethyl acetate, a low toxicity and greener solvent, and the development of processes at room temperature, thus avoiding energy consumption and avoiding loss of temperature sensitive or volatile components (Calderó et al 2011 and 2016; Vílchez et al. 2014; Leitner et al. 2019). In addition, this approach does not require sophisticated equipment such as high shear stirrers, high pressure homogenizers or ultrasound generators.

In most applications, size and surface charge are of special interest. It is well known that nanometric sizes provide materials with new physicochemical and functional properties (optical, magnetic, biological, etc.) which are not present in bulk. Both, size and surface charge have been described to influence the stability of the dispersed systems, their toxicity, biodistribution, etc. (He et al. 2010; Jiang et al. 2009). In particular, positive surface charge imparts interesting properties which are used for example for drug or gene delivery or to provide mucoadhesive, antimicrobial, antifouling or decontaminant properties (Qi et al. 2004; Chang et al. 2015; Kim et al. 2018; Lin et al. 2017). Interestingly, even though ethylcellulose is a nonionic polymer, it has been generally reported to display negative surface charge (Gunduz et al. 2013; Balzus et al. 2017; Hayden et al. 2018; Božič et al. 2018). In order to provide ethylcellulose-based materials with a positive surface charge, several strategies have been proposed e.g. physical mixtures with other cationic polymers like ammonium methacrylate copolymer type B (Balzus et al. 2017) or covalent grafting of cationizable chains to the ethylcellulose backbone (Wanga et al. 2011). Recently, we have reported the formation of cationic ethylcellulose nano-emulsions and nanoparticles by the PIC approach in a Water / surfactant mixture / ethylcellulose solution system at room temperature (Leitner et al. 2019). The surfactant mixture consisted of a cationic alkylamidoammonium derivative and a nonionic sorbitan ester (Span 80). The obtained ethylcellulose template nano-emulsions and nanoparticles displayed zeta potential values as high as 55 mV. However, their sizes were rather large (close to 300 nm). In addition, the relation of size, surface charge and colloidal stability with composition variables had not been studied in depth. In the present work, we investigate systematically the relation of the nano-

emulsion template composition with the characteristics of both, the nano-emulsion and the nanoparticles obtained from them in a similar cationic-nonionic surfactant system, in which the sorbitan ester has been replaced by an ethoxylated fatty acid ester of low hydrophilic-to-lipophilic balance (HLB), with the aim of achieveing smaller mean nanoparticle sizes.

The goal of this research is to gain new knowledge on the impact of composition variables such as the oil-to-surfactant ratio, the cationic-to-nonionic surfactant ratio or the water content on the size and surface charge of template nano-emulsions prepared using a low-energy emulsification approach and nanoparticles obtained from them, with the aim of providing valuable tools for the control and prediction of these characteristics.

2. EXPERIMENTAL

2.1. Materials

Ethylcellulose polymer (ETHOCEL Premium Std 10, Dow Chemical Company, abbreviated as EC10) a commercial semi synthetic cellulose ether derivative, insoluble in water, was kindly donated by Colorcon, a distributor of the Dow Chemical Company. Ethylcellulose consists of repeating anhydroglucose units in which hydroxyl groups have been partially substituted by ethoxyl groups. Ethoxyl content was 48.7% and the weight-average molecular weight (Mw) was 66385 ± 322 Dalton with a polydispersity of 4.3 as determined by Gel Permeation Chromatography. Details on the analysis are reported elsewhere (Leitner et al. 2019). Ethyl acetate (> 99.8%, Merck) was used as organic solvent. This solvent has a boiling point of 77ºC. It is soluble up to around 7.7 wt% in water and can dissolve 3.3 wt% water at 25 ºC (Calderó et al. 2011 and 2016). The cationic surfactant was a ricinoleamidopropyltrimonium methosulfate (abbreviated as Cat A; **Figure 1**) from Evonik, with an active matter content of 40 wt% in water and a critical micellar concentration of 3.3 x 10^{-2} mM (Burgos-Mármol et al 2016). The nonionic surfactant was PEG-7 hydrogenated castor oil

(Cremophor WO7, from BASF; abbreviated as CWO7), whose HLB number is 5 ± 1 (Kolliphor Technical Information 2014). Water was deionized and MilliQ® filtered.

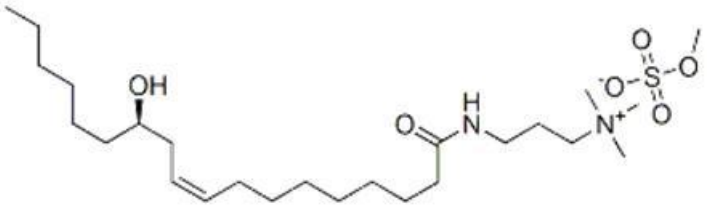

Figure 1: Chemical structure of ricinoleamidopropyltrimonium methosulfate (Cat A).

2.2. Methods

2.2.1. Preparation of oil-in-water (O/W) nano-emulsions

About 6 g of the nano-emulsions were prepared in a 10 mL test tube, at a constant temperature of 25°C by adding water drop-wise to the mixture of the ethylcellulose solution (from now on referred as “oil”) and previously homogenized surfactants. The addition was performed under permanent vortex stirring (Vortex Genie 2, Scientific Industries Inc.) at about 2700 rpm, keeping the test tube closed with a septum to avoid solvent evaporation. The addition of the water was carried out through the septum, with the help of a peristaltic pump (Watson Marlow 323 Pump) and UPS Class VI silicone tubing (internal diameter of 0.8mm) fitted to a G18x1 ½” needle, at a constant rate of 0.05gwater/second.

2.2.2. Nano-emulsion domain determination

The region of formation of O/W nano-emulsions in the Water / [cationic:nonionic surfactant mixture] / [EC10 in ethylacetate] system was at first assessed visually at 25°C. Samples with various O/S ratios and water contents were prepared as described in **Section 2.2.1**. Compositions with a transparent or translucent appearance and a reddish or bluish shine when observed through a lamp light were identified as nano-emulsions.

2.2.3. Phase Inversion determination

The phase inversion region was determined by conductivity measurements. Samples (4 g) were prepared by addition of water to oil/surfactant mixtures up to 95 wt%. Electrical conductivity of samples was measured at each composition by means of a Crison-GLP 31 conductimeter with a Pt/platinized electrode under continuous magnetic stirring at 25ºC.

2.2.4. Nanoparticle preparation

Nanoparticles were prepared by the solvent evaporation method using a rotary evaporator (Büchi) during 45 minutes under reduced pressure of 43 mbar and at 25°C to achieve ethyl acetate removal to below 5000 ppm residual solvent as determined by gas chromatography. After evaporation, weight loss was replaced with water.

2.2.5. Particle size characterization

The mean size of nano-emulsion droplets and nanoparticles was determined by dynamic light scattering (DLS) measurements performed on a 3D cross-correlation spectrometer (LS Instruments) equipped with a He-Ne laser (λ=632.8 nm), and a modulator for concentrated samples, suitable for the sizing of particles from 0.5 nm to 5 µm. This cross-correlation technology suppresses multiple scattering effects and allows performing the measurements of the samples as prepared, without further dilution. Analysis of each composition was carried out in triplicate on at least two independent samples. Measurements were performed on a 3 mL square cell, at a scattering angle of 90° and a temperature of 25 °C. Dynamic light scattering data were treated by cumulant analysis to obtain the mean hydrodynamic diameter (Pecora et al. 2000; Brown 1993). Refractive indexes and viscosity data required for DLS analysis were determined experimentally (please, see **Supplementary Information 1**). The refractive indexes of the continuous phases were 1.3358 ± 0.0002 for the nano-emulsions and 1.3334 ± 0 for the nanoparticle dispersions. Viscosities of the continuous phases were 1.005 ± 0.026 cP for the nano-emulsions and 0.937 ± 0.006 cP for the nanoparticle dispersions.

2.2.6. Nano-emulsion and nanoparticle dispersion stability

Nano-emulsion and nanoparticle dispersion stability was assessed both, by visual observation of phase separation at a constant temperature and by light backscattering measurements. For the visual assessment, nano-emulsions and nanoparticle dispersions were kept in a glass vial in a thermostated bath at 25°C and checked as a function of time. They were considered stable when no macroscopic phases were observed.

Nano-emulsion stability was also assessed from multiple light scattering measurements by means of a Turbiscan Lab Expert at constant temperature (25ºC) and λ=880nm. For this purpose, 15g of nano-emulsion were filled, immediately after preparation, in a glass measurement cell which was tightly stoppered to avoid solvent evaporation. Transmission and backscattering data were acquired at 180º and 45º respectively from the incident beam for 24 hours at intervals of 1 hour.

2.2.7. Nano-emulsion and nanoparticle surface charge

The zeta potential, a measure of the net surface charge, was determined from the electrophoretic mobility measured on a ZetaSizer Nano Z laser diffractometer (Malvern Instruments) by applying the Smoluchowsky equation:

$$\mu = \frac{\zeta\, \varepsilon_r\, \varepsilon_0}{\eta}$$

where μ is the electrophoretic mobility, ζ is the zeta potential, ε_r is the dielectric contrant of the medium, ε_0 is the dielectric constant of the vacuum and η is the viscosity of the medium (Delgado et al. 2007). For the measurements, nano-emulsions and nanoparticles dispersions were diluted with water to a concentration of 20 mg nano-emulsion/g solution. Each sample was measured in triplicate at room temperature.

2.2.8. Shrinking factor determination

The shrinking factor upon nanoparticle formation from the nano-emulsion droplets was determined as the ratio between the volume of the template nano-emulsion droplet and the volume of the nanoparticle formed. For the calculation

of the respective volumes, the mean hydrodynamic radii, as determined by DLS (see section 2.2.5.) are used.

$$f = \frac{V_{NE}}{V_{NP}} = \frac{{}^{4}/_{3}\ \pi\ r_{NE}^{3}}{{}^{4}/_{3}\ \pi\ r_{NP}^{3}} = \frac{r_{NE}^{3}}{r_{NP}^{3}}$$

where *f* is the shrinking factor; V_{NE} and V_{NP} are the volumes of a nano-emulsion drop and a nanoparticle respectively; r_{NE} and r_{NP} are the mean hydrodynamic radii or the nano-emulsion and the nanoparticle dispersion, as determined by DLS. Data are interpreted considering that no droplet size change due to coalescence, Ostwald ripening or flocculation occurs during solvent evaporation and that each single nano-emulsion drop generates one nanoparticle. A shrinking factor of 1 would mean no volume reduction of the template nano-emulsion droplet to form the nanoparticle, thus indicating that no significant amount of ethyl acetate is present in the dispersed phase of the nano-emulsion.

2.2.9. Dialysis experiments

Dialysis experiments were performed to determine the desorption kinetics of CatA from the nanoparticles by means of conductivity and zeta potential measurements. For this purpose, about 8 g of nanoparticle dispersion were filled in a SpectraPor dialysis bag (MWCO of 12000 – 14000) and immersed in 2000 mL of MilliQ filtered water at 25ºC. The conductivity in the nanoparticle dispersion was monitored by means of a Crison-GLP 31 conductimeter with a Pt/platinised electrode. Conductivity data were automatically collected on a computer along the experimental time. For zeta potential measurements, an aliquot of the nanoparticle dispersion was withdrawn from the dialysis bag and measurements were performed as explained in section **2.2.7**.

3. RESULTS AND DISCUSSION

3.1. O/W ethylcellulose nano-emulsion formation in the Water / [CatA:CWO7] / [EC10 in ethyl acetate] system at 25ºC

O/W nano-emulsion formed by the phase inversion composition (PIC) method has been studied in the Water / [CatA:CWO7] / [6% EC10 in ethyl acetate] system at 25ºC, at CatA:CWO7 ratios of 1:1 and 1:3. It has been found that O/W nano-emulsions form at both surfactant ratios tested in the same oil-to-surfactant (O/S) range and water contents (**Figure 2a**). Nano-emulsions form close to the water vertex of the pseudoternary diagram, at O/S ratios comprised between 55/45 and 75/25 and above 88 wt% water as assessed by visual observation. It is worth mentioning that no nano-emulsions are formed in the absence of nonionic surfactant, that is, in the Water / CatA / [6% EC10 in ethyl acetate] system at 25ºC. In contrast, O/W ethylcellulose nano-emulsions are formed by the phase inversion composition method in systems containing only nonionic surfactants, of the ethoxylated sorbitan ester type (Spernath et al 2007) and the ethoxylated fatty alcohol type (Calderó et al. 2016) with HLB values typically between about 12 and 14. However, as shown in this study, nano-emulsions can be obtained by mixing CatA with an ethoxylated fatty acid derivative (CWO7) with a hydrophilic to lipophilic balance (HLB) value of about 5. By fixing the oil-to-surfactant ratio (O/S) at 70/30 and varying the CatA:CWO7 ratio, nano-emulsions are formed in the CatA:CWO7 span between 1:1 and 1:8.

The nano-emulsion domain of the Water / [CatA:CWO7=1:1] / [6% EC10 in ethyl acetate] system is smaller than that described recently in the Water / [CatA:Span80 = 1:1] / [6% EC10 in ethyl acetate] system at 25ºC (Leitner et al 2019). These systems differ only in the nonionic surfactant. Although the HLB values of these nonionic surfactants are quite close, they differ in their chemical structure as Span 80 is a non-ethoxylated sorbitan ester with an HLB value of 4.3. Concerning the size of the nano-emulsion domain it may be inferred that Span 80 is a more favorable nonionic surfactant for nano-emulsion formation in this kind of system. However, as will be shown later, smaller droplet sizes are attained with CWO7.

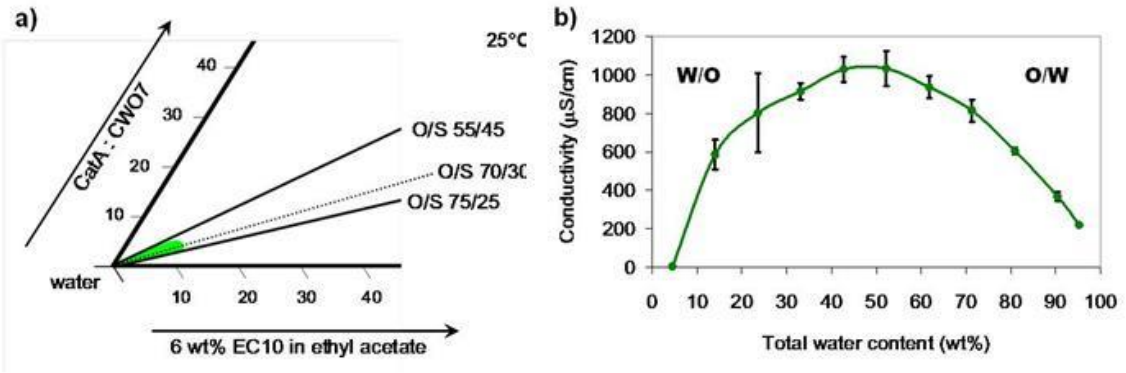

Figure 2: a) Oil-in-water (O/W) nano-emulsion domain (green area) in the Water / [CatA:CWO7] / [6%EC10 in ethyl acetate] system for CatA:CWO7 ratios of 1:1 and 1:3 at 25ºC. The O/W nano-emulsion domains are coincident for both CatA:CWO7 tested (1:1 and 1:3) and are therefore reported in a single diagram; b) Conductivity as a function of total water content in the Water / [CatA:CWO7 = 1:3] / [6 wt% EC10 in ethyl acetate] system along the dilution path with the O/S ratio of 70/30, at 25ºC. Water-in-oil (W/O) and oil-in water (O/W) regions are indicated.

Conductivity measurements were carried out in order to assess if a transition from W/O to O/W structures took place during emulsification. **Figure 2b** illustrates the conductivity values of a sample at an O/S ratio of 70/30 and increasing water content at 25ºC. No conductivity values could be obtained below 5 wt% water due to the water already present in CatA as mentioned above. Conductivity values of samples with around 25 wt% water fluctuated due to their instability which could be indicative of phase transition. Conductivity values increase with the increase of water content, reaching a maximum and then gradually decrease due to the effect of dilution of the conducting species. Conductivity reaches values as high as about 1000 µS/cm, much higher than those obtained with a similar system prepared only with nonionic surfactant (typically below 400 µS/cm if the aqueous component is water) (Calderó et al 2011 and 2016). The phase inversion takes place around 30 wt% water.

It was also considered of interest to determine the effect of a higher polymer concentration in the nano-emulsion domain. For this purpose, the EC10 concentration in the oil component was increased up to 10 weight % keeping

the CatA:CWO7 ratio at 1:3. At this higher polymer concentration, nano-emulsions were formed between O/S ratios of 65/35 and 75/25 and above 88 wt% of water. This can be interpreted in terms that higher polymer concentrations do not favour the formation of nano-emulsions at this cationic:nonionic surfactant ratio.

3.2. Influence of composition variables on the size of ethylcellulose nano-emulsions and nanoparticles

Nano-emulsions with a water content of 90 wt% and 95 wt% were selected for further characterization. Droplet sizes, obtained by DLS, are below 200 nm, and do not differ much when increasing the water content from 90 to 95 wt% as shown in the blue dotted graphs in **Figures 3a** and **3b**. Although one might expect an increase in the O/W nano-emulsion droplet size at increasing oil content, this is not evident in **Figure 3**. At 90 wt% water content and O/S ratios between 60/40 and 70/30 droplet size first remains roughly constant and then increases at the O/S ratio of 75/25. This may be explained by the solvent diffusion from the droplets to the continuous phase due to the partial solubility of ethyl acetate in the aqueous component, counteracting the expected droplet size increase. As mentioned in the experimental section, ethyl acetate is partially soluble up to about 7.7 wt % in water at 25 ºC (Calderó et al. 2011 and 2016). At the higher O/S ratios the dispersed phase fraction effect would dominate over the diffusion effect, producing a droplet size increase (**Figure 4**). This trend is more noticeable at 95 wt% water content which may be due to the larger ethyl acetate diffusion at already low O/S ratios and the lower overall surfactant content as compared to the nano-emulsions with 90 wt% water. The observed behaviour is different from that described in systems with less polar oils where no or very low diffusion of the dispersed phase is produced and hence the droplet diameter increases with increasing O/S ratio (Sadurní et al 2005). At 90 wt% water content the smallest droplet size was attained at O/S ratio of 65/35 with a mean hydrodynamic diameter of about 125 nm, while the largest droplet diameter was attained at an O/S ratio of 75/25 (close to 154 nm). At 95 wt% water content and an O/S ratio of 75/25, the nano-emulsion mean droplet size is considerably larger than that of the nano-emulsion with 90 wt%

water, reaching a mean hydrodynamic diameter of 174 nm, while the smallest sizes are attained at O/S ratios of 60/40 and 65/35 (around 118 nm). Although it might be expected that nano-emulsion droplet sizes are similar for water contents of 90 and 95 wt%, several factors such as solvent diffusion from the nano-emulsion drops to the continuous phase, overall surfactant content in the nano-emulsion, surfactant hydration or polymer chain folding may play a role in the mean droplet diameter. In spite of the fact that the nano-emulsion formation region of the system with the here described surfactant mixture CatA:CWO7 is smaller than that of the system with the surfactant mixture CatA:Span80 = 1:1 reported recently (Leitner et al, 2019), it is worth mentioning that droplet sizes in CatA:CWO7 are half as big as those of the emulsions obtained at the same O/S ratios with CatA:Span80, suggesting that CatA:CWO7 mixtures may form more compact interfacial films.

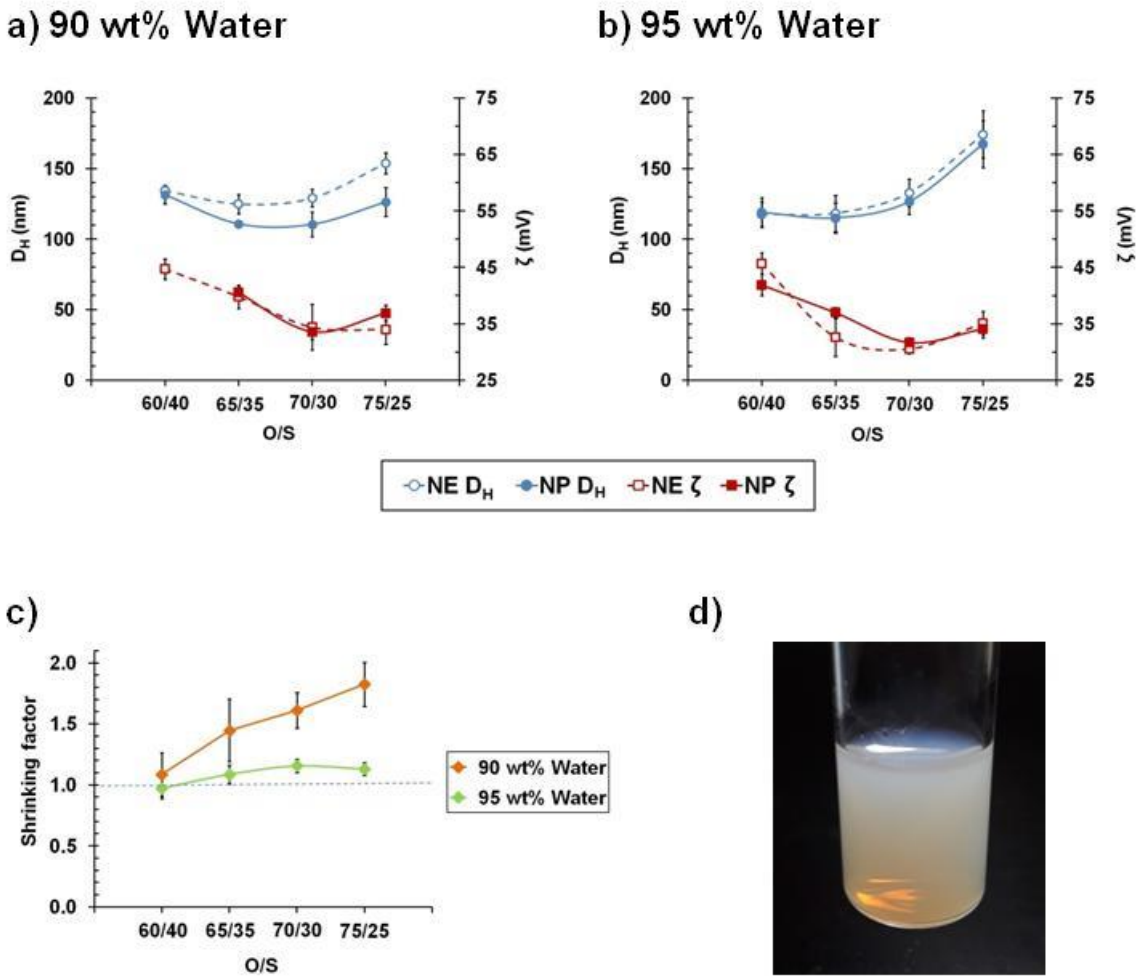

Figure 3: Diameter (D_H; in blue colour) and zeta potential (ζ, in red colour) as a function of the oil-to-surfactant ratio (O/S) of the nano-emulsions (dotted lines)

and the nanoparticle dispersions (solid lines) obtained from nano-emulsions by solvent evaporation in the Water / [CatA:CWO7 = 1:3] / [6 wt% EC10 in ethyl acetate] system with a) 90 and b) 95 wt% water content, at 25ºC. c) Shrinking factor of the nano-emulsions with 90 and 95 wt% water content upon nanoparticle formation by solvent evaporation. d) Visual appearance of a representative nanoparticle dispersion sample of the Water / [CatA:CWO7 = 1:3] / [6 wt% EC10 in ethyl acetate] system prepared from a nano-emulsion template with an O/S ratio of 65/35 and 95 wt% water content. The sample shows a slightly translucent appearance with a reddish shine due to the scattering of incident light (Tyndall effect).

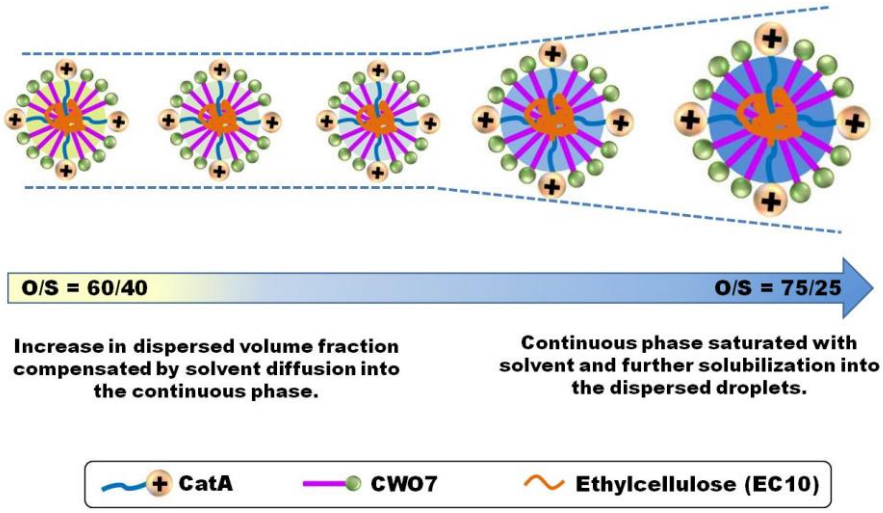

Figure 4: Schematic illustration of the influence of the oil-to-surfactant ratio (O/S) in the droplet size at a fixed CatA:CWO7 ratio.

The influence of the CatA:CWO7 ratio in the droplet size of the nano-emulsion has also been investigated by keeping the O/S ratio constant at 70/30. The CatA:CWO7 ratios tested have been 1:1, 1:3, 1:4, 1:6 and 1:8. Hydrodynamic diameters of the nano-emulsion droplets (NE) and the nanoparticles (NP) obtained from them are displayed in **Figure 5a** (90 wt% water content) and **Figure 5b** (95 wt% water content). As for the nano-emulsions, at both water contents (NE 90% and NE 95%), the droplet size as a function of CatA:CWO7 ratio follows a parabolic profile with lowest mean droplet size values at 1:3 and 1:4 ratios. At higher CatA content in the surfactant mixture (e.g. CatA:CWO7 = 1:1), electrostatic repulsion between the charged head-groups of CatA molecules is expected to be higher at the interfacial film of the droplet, favoring the formation of large droplets (**Figure 6**, left image). It is worth recalling that in

the absence of nonionic surfactant (that is, CatA:CWO7 = 1:0) no nano-emulsions are formed. When decreasing the CatA:CWO7 ratio to 1:3 and 1:4, electrostatic repulsion at the interfacial film of the droplets decreases, allowing the hydrocarbon tails of the surfactant molecules to further approach each other favoring hydrophobic interactions and optimal tight interfacial film packing as schematically drawn in **Figure 6**. When further increasing the nonionic surfactant proportion to CaA:CWO7 = 1:8, droplet swelling and hence droplet size increase may occur. This may be attributed to a change in the effective cross-sectional area per surfactant molecule. Rodriguez et al. (Rodríguez et al 2004) reported that in mixed nonionic/cationic surfactant aqueous systems the effective cross-sectional area per surfactant molecule significantly decreases with the addition of nonionic surfactant in cationic surfactant systems. It may be inferred that a similar effect may take place when decreasing the CatA:CWO7 ratio from 1:3 to 1:8.

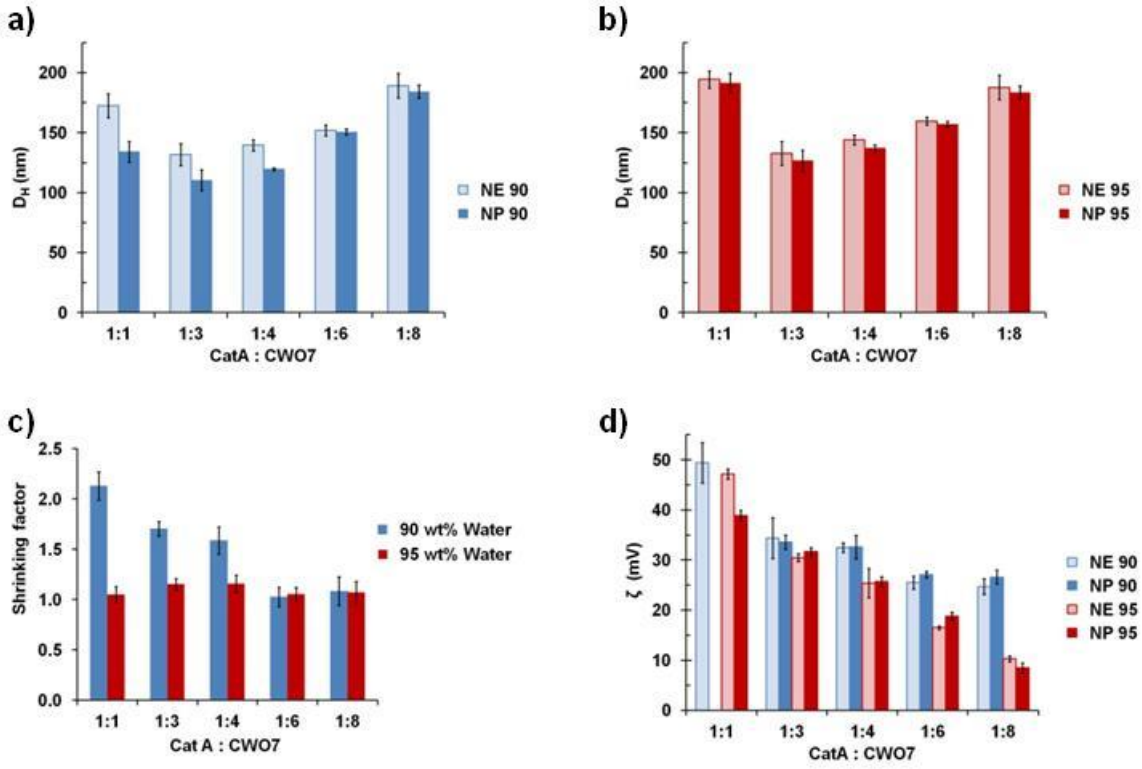

Figure 5: Hydrodynamic diameter (a and b), shrinking factor (c) and zeta potential (d) of nano-emulsions with 90 wt% (NE 90) and 95 wt% (NE 95) water, formed in the Water / [CatA:CWO7] / [6% EC10 in ethyl acetate] system at varying CatA:CWO7 ratios at 25ºC, and of the nanoparticle dispersions obtained from the nano-emulsions.

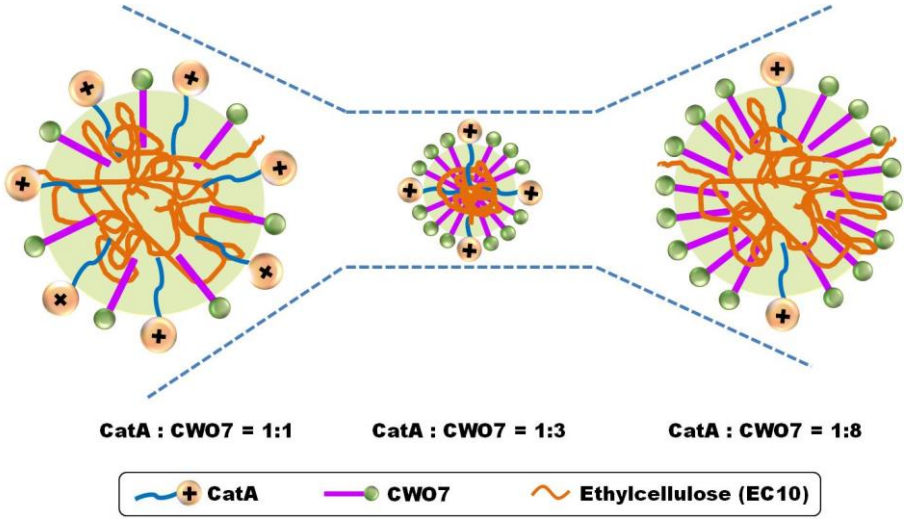

Figure 6: Schematic illustration of droplet size change as a function of CatA:CWO7 surfactant ratio.

Table I shows the comparative values of droplet size of nano-emulsions with 6% and 10% EC10 and a water content of 90 and 95 wt%. Nano-emulsions containing 10 wt% polymer have droplet sizes larger than corresponding nano-emulsions prepared with 6 wt% polymer in the oil component at both water contents. This can be explained by the fact that at higher polymer concentration swelling of the droplet may occur. All nano-emulsions show polydispersity indices around 0.4.

Table I: Nano-emulsion droplet diameter (D_H) with polydispersity index (PI) as determined by DLS, zeta potential (ζ) and stability assessed visually of nano-emulsions with an O/S ratio of 70/30 of the Water / [Cat A:CWO7 = 1:3] / [X wt% EC10 in ethyl acetate] system as a function of polymer concentration in the oil component, at 25ºC.

wt% EC10 in the oil	wt% water in the NE	D_H (nm)	ζ (mV)	Stability (days)
6	90	129.2 ± 6.2	34.4 ± 4.0	66
	95	132.8 ± 9.8	30.5 ± 0.8	70.5
10	90	141.2 ± 4.7	25.9 ± 1.1	3
	95	140.9 ± 12.5	23.1± 0.6	3

The nano-emulsions were used for nanoparticle preparation by ethyl acetate evaporation under reduced pressure as explained in the experimental section. As shown in **Figures 3** and **Figure 5** (in both Figures, graphs a and b) the nanoparticles show generally smaller sizes than the template nano-emulsions and a variation trend close to that of their template nano-emulsions. **Figure 3d** shows the typical visual appearance of a nanoparticle dispersion in these systems. The size of the nanoparticles obtained from the nano-emulsions with 90 wt% water content as a function of the studied O/S ratio (**Figure 3a**) ranges from about 110 nm to about 130 nm, while the nanoparticles obtained from nano-emulsions with 95% water content range from 115 nm to about 170 nm.

An interesting parameter is the shrinkage of the nano-emulsion droplet for nanoparticle formation. **Figure 3c** shows the shrinking factor (determined as explained in section 2.2.8) of the studied nano-emulsions as a function of the O/S ratio. It is shown that for nano-emulsions with a 90 wt% water content and a fixed CatA:CWO7 ratio of 1:3, the experimental shrinking factor is close to 1 at an O/S ratio of 60/40, while at O/S ratios above 65/35 the shrinking factor increases almost linearly up to 1.8. This is reasonable as the ethyl acetate content in the nano-emulsion with an O/S ratio of 60/40 is about 5.6 wt% and this amount may be almost completely diffused from the droplet to the continuous phase to reach equilibrium. However, at O/S ratios above 65/35, the ethyl acetate content in the nano-emulsion is higher than 6 wt%. Although this amount is below the saturation concentration in water (around 7.7 wt%), the surfactant interfacial film may be able to retain this solvent inside the droplet. At 95 wt% water content, the shrinking factor keeps close to unity regardless the O/S ratio indicating that droplet volume reduction for nanoparticle formation is minimal. This is consistent with the fact that the amount of ethyl acetate in the nano-emulsions with 95 wt% water content is below 3.5 wt% in the O/S ratio range studied. These results suggest that saturation of the aqueous phase of these nano-emulsions is attained around 6 wt% of ethyl acetate.

Concerning the influence of the CatA:CWO7 ratio, at a fixed O/S ratio of 70/30, particle sizes are typically between 110 and 185 nm for those prepared from nano-emulsions with 90 wt% water content and between 125 nm and 190 nm

for those prepared from nano-emulsions with 95 wt% water content. In the studied CatA:CWO7 range, the minimum nanoparticle size is attained at a CatA:CWO7 ratio of 1:3.

The analysis of the shrinking factor reveals that when keeping the O/S ratio constant at 70/30 and a 90 wt% water content, the shrinking factor decreases with the CatA:CWO7 ratio from about 2 at a CatA:CWO7 ratio of 1:1 to a value of around 1 at a CatA:CWO7 ratio of 1:6, and does not change when further decreasing this ratio down to 1:8 (**Figure 5c**). This suggests that at higher Cat A content the interfacial film is more impermeable to ethyl acetate diffusion and/or that equilibrium concentration in the aqueous phase of the nano-emulsion is lower. At a 95 wt% water content however, shrinking factor remains close to 1 regardless the CatA:CWO7 ratio, which may be explained by the low ethyl acetate content present in the nano-emulsion.

3.3. Influence of composition variables on the surface charge of ethylcellulose nano-emulsions and nanoparticles

Due to the presence of the cationic surfactant, the surface charge of the nano-emulsion droplets and the nanoparticles obtained from them in the Water / CatA:CWO7 / [EC10 in ethyl acetate] systems studied in this work is expected to be positive. However, it is noteworthy to recall that ethylcellulose nano-emulsions and nanoparticles show typically negative surface charge, generally in the range of -20 mV to -30 mV (Hayden et al 2018; Balzus et al 2017; Obst et al 2017; Mimi et al 2015).

The zeta potential of the nano-emulsions and nanoparticles studied are displayed (red graphs) in **Figures 3a** and **3b**. As expected, the zeta potential values of these systems are positive and vary between about 30 mV and about 45 mV, depending on the O/S ratio. The degree of dilution (i.e., 90 wt% or 95 wt% water) does not exert a significant influence in the zeta potential value. It is worth mentioning that the zeta potential values of nano-emulsions with 10 wt%

polymer are about 10 mV lower than those with 6 wt% (**Table I**). This may be due to a more dense distribution of polymer and shielding at the droplet surface, causing a reduced possibility for the cationic surfactants to place themselves at this site.

As for the influence of the CatA:CWO7 ratio on the zeta potential values, there is an increase with increasing CatA:CWO7 ratio. This trend can be observed for both water contents, although as expected, zeta potential values are higher in nano-emulsions with 90 wt% water. Nano-emulsions and nanoparticles with CatA:CWO7 ratio 1:1 show values as high as about +50 mV with both, 90 and 95 wt% of water. This value is of the same order than that obtained in the system with Span 80 as the nonionic surfactant at the same O/S ratio and CatA:nonionic surfactant ratio and 90 wt% water (Leitner et al 2019). At decreasing CatA:CWO7 ratios, zeta potential values of the nano-emulsions also decrease, being the values lower at the higher water content. Thus, as shown in **Figure 5d**, the zeta potential value of the nano-emulsion with 95% water content and CatA:CWO7 ratio of 1:8 displays a zeta potential of only +10.3 mV. At high CatA:CWO7 ratios the zeta potential of nano-emulsions with 90 and 95 wt% water are quite close to each other, and the difference among them increases with decreasing CatA:CWO7 ratios. Zeta potential values of the nanoparticles are comparable and do not differ significantly from those of the template nano-emulsions for varying O/S ratios (**Figures 3a and 3b**). Also, as observed for corresponding nano-emulsions, the zeta potential for the nanoparticle dispersions decreases with decreasing CatA:CWO7 ratio due to the decreasing amount of cationic surfactant (**Figure 3b**). It is noteworthy that the nanoparticle dispersions prepared from the nano-emulsions with 95% water content and CatA:CWO7 ratios of 1:1 and 1:8 show similar mean hydrodynamic diameters (around 185 nm) but their zeta potential values differ in about 30 mV (38.9 ± 1.0 mV and 8.5 ± 1.0 mV respectively).

These zeta potential values obtained in the tested compositions are high enough to impart electrostatic stabilization to the dispersed nano-emulsion droplets and nanoparticles as generally accepted for zeta potential values equal or above 25 mV (Hertault et al 2003). In addition, they are comparable to the

zeta potential values attained when mixing ethylcellulose polymer with other cationic polymers. For example, polymeric nanoparticles prepared with a mixture of ethylcellulose and ammonium methacrylate copolymer type B at a ratio of 1:1 show zeta potential values of 34 mV (Balzus et al 2017). Nanocarriers prepared with the cationic polysaccharide chitosan, either complexed with tripolyphosphate (TPP) or functionalized with organosilane, have been reported to have zeta potential values around 20 mV (Giarra et al 2018; Kashkouli et al 2019) while cationic liposomes may reach zeta potential values in the range between 34 mV and 41 mV depending on the lipid composition (Smith et al 2017; Monpara et al 2019). This confirms that the strategy proposed here allows reaching zeta potential values in a comparable range.

An important issue from an applicative point of view is the desorption kinetics of the cationic surfactant when exposed to a diluting medium. To investigate this aspect, the nanoparticle dispersion obtained from the nano-emulsion of the Water / [CatA:CWO7 = 1:3] / [6 wt% EC10 in ethyl acetate] system with an O/S ratio of 70/30 and 95 wt% water content was dialysed against an excess of receptor solution (water) at a constant temperature of 25ºC. The conductivity and zeta potential data of the nanoparticle dispersion were collected as a function of time. It is observed that the conductivity of the nanoparticle dispersion displays a strong decrease during the first hours of dialysis (**Figure 7**) and reaches a plateau after a period of about 24 hours. The zeta potential values however, denote a slow drop of surface charge from positive (+30.5 mV) to negative values after about 50 hours dialysis. A stable value of about -20 mV is reached after about one week of dialysis (**Supplementary Information 2**). During the first 24 hours of dialysis, the zeta potential drops to about its half, but keeps positive values. This suggests that during the first hours of dialysis the excess CatA surfactant, which is not adsorbed on the nanoparticle surface, may diffuse fast to the receptor solution, which would explain the sharp decrease of conductivity within the first hours in the nanoparticle dispersion. However, the CatA adsorbed on the nanoparticle surface is desorbed more slowly as shown by the smooth zeta potential decrease, so that only after about one week of dialysis an equilibrium negative value is reached, indicating that most CatA may

have been desorbed by then from the surface of the nanoparticles. Interestingly, in contrast to other cationic nanosystems, these results may indicate that under diluting conditions in an aqueous medium, the positive surface charge of the nanoparticles is time-dependent and can be gradually depleted until reaching a negative plateau value close to that of ethylcellulose nanoparticles without CatA.

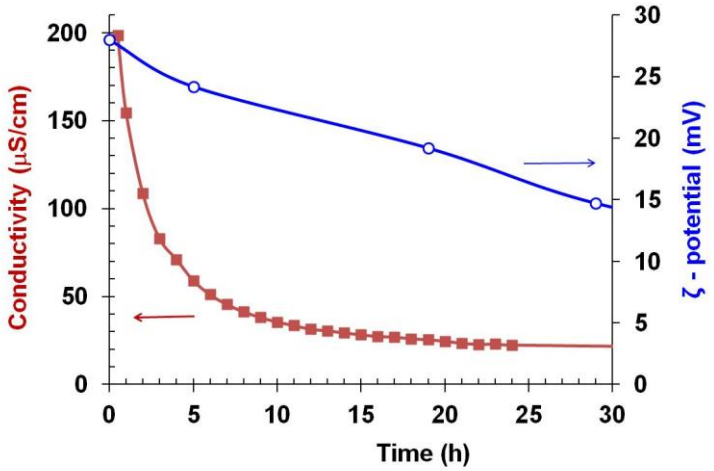

Figure 7: Conductivity and zeta potential values of the nanoparticle dispersion as a function of time, measured during dialysis of the nanoparticle dispersion obtained from a nano-emulsion of the Water / [CatA:CWO7 = 1:3] / [6 wt% EC10 in ethyl acetate] system with an O/S ratio of 70/30 and 95 wt% water content.

3.4. Influence of composition variables on the colloidal stability of ethylcellulose nano-emulsions and nanoparticles

Colloidal stability is an important feature of dispersed systems for both, storage and applicative reasons. It is expected that smallest droplet (and particle) sizes provide improved stability against sedimentation and creaming, while high enough zeta potential values have been related to an enhanced stability against flocculation and coalescence, owing to electrostatic repulsion among droplets having charges of the same sign.

A preliminary visual stability assessment of the nano-emulsions and nanoparticle dispersions at a constant temperature of 25ºC was carried out as

explained in the experimental section. **Figure 8a** shows that stability might be optimal at an O/S ratio of 70/30. This may be related to the small droplet size of the nano-emulsions at this O/S ratio, which reduces droplet migration phenomena. It is worth mentioning that nano-emulsions with O/S ratios of 65/35 and 70/30 achieve around 2 months of stability, regardless the water content is 90 or 95 wt%. Concerning the role of the polymer concentration, as shown in **Table I**, nano-emulsion stability at a fixed O/S ratio of 70/30 and CatA:CWO7 ratio of 1:3 is significantly lower with 10 wt% EC10 in the oil component than with 6 wt%. The lower stability of the nano-emulsions with 10% EC content in the oil component may be due to the joint contribution of several factors, including the larger size, the higher density and the lower zeta potential of the droplets in the nano-emulsions with 10% EC10 in the oil component. Larger sizes and higher density of the dispersed droplets accelerate the destabilization phenomena due to migration of the droplets (e.g. sedimentation). The increased density is due not only to the higher polymer content (its density is 1.32 g/cm^3) but also to the lower ethyl acetate (0.9 g/cm^3) content in the droplets with 10 wt% EC10. Another factor contributing to lower stability of nano-emulsions with 10% EC10 content in the oil component may be the lower electrostatic repulsion, as expected from the lower zeta potential values obtained in these emulsions.

Figure 8b shows the visual stability as a function of CatA:CWO7 ratio of nano-emulsions and nanoparticle dispersions prepared with 90 and 95 wt% of water. The preliminary visual assessment of the stability of the studied nano-emulsions as a function of CatA:CWO7 ratio suggests that in general terms, the highest stability is attained at CatA:CWO7 ratios of 1:3, regardless the water content of the nano-emulsion. These nano-emulsions are stable for a period of around or above 2 months. It can be noticed that there is not a direct correlation between the electrostatic stability predicted through high zeta potential values and the actual visually observed stability. The nano-emulsions with the CatA:CWO7 ratio 1:1 show visual stabilities of maximum about 2 days in spite of having the highest zeta potential values. In most of the samples, the occurring instability was sedimentation. It is worth recalling that for such droplet/particle migration phenomena, size has a predominant role as described in Stokes equation of sedimentation velocity. Theoretical calculations considering experimental

droplet size data confirm that highest stability against droplet migration phenomena is expected for nano-emulsions with CatA:CWO7 ratios of 1:3 and 1:4 (**Supplementary information 3**). From the overall size, zeta potential and stability data, it can be concluded that the most suitable CatA:CWO7 ratio is 1:3, as at this ratio smallest droplet sizes, high zeta potential values and optimal stability are attained.

When comparing nano-emulsion templates with their corresponding nanoparticle dispersions, the preliminary visual assessment suggests that nanoparticle dispersions show generally lower stability (**Figures 8a and 8b**). An explanation to this observation may be an increased tendency to sedimentation due to the higher density of the nanoparticles as compared to the nano-emulsion drops. Although other factors may be also involved in the observed increased instability of the nanoparticle dispersions, such as for example flocculation, these factors have not been studied yet in detail.

In order to know better the mechanisms of destabilization, the stability of the nano-emulsions was assessed also by measuring the backscattering intensity as a function of time and sample height. **Figure 8c** displays the light backscattering spectrum of the nano-emulsion with an O/S ratio of 70/30, which is quite representative of the general behaviour of the nano-emulsions of this system. As shown, backscattering intensity decreases with time all along the sample height, though backscattering spectra keep parallel. It should be noticed that the sharp backscattering and transmission changes at the bottom of the cell and/or the meniscus of the sample (highlighted in grey) have no physical meaning. The backscattering decrease may be attributed to the clarification of the continuous phase caused by either a decrease in size according to diffusion of ethyl acetate from the droplets to the continuous phase or by a decrease in number of droplets as a consequence of coalescence, flocculation or Ostwald ripening. However, it can also be noticed that the change is only in a minor degree (backscattering intensity drop of about 2% from initial 17% to about 15%). The parallel pattern of backscattering spectra denotes that the nano-emulsion stays homogeneous over the whole sample height, that is, no significant sedimentation or creaming takes place during the analysis time (the

first 24 hours). Thus, nano-emulsions with this backscattering pattern can be considered as relatively stable during measurement time and appropriate to be used as templates for nanoparticle preparation.

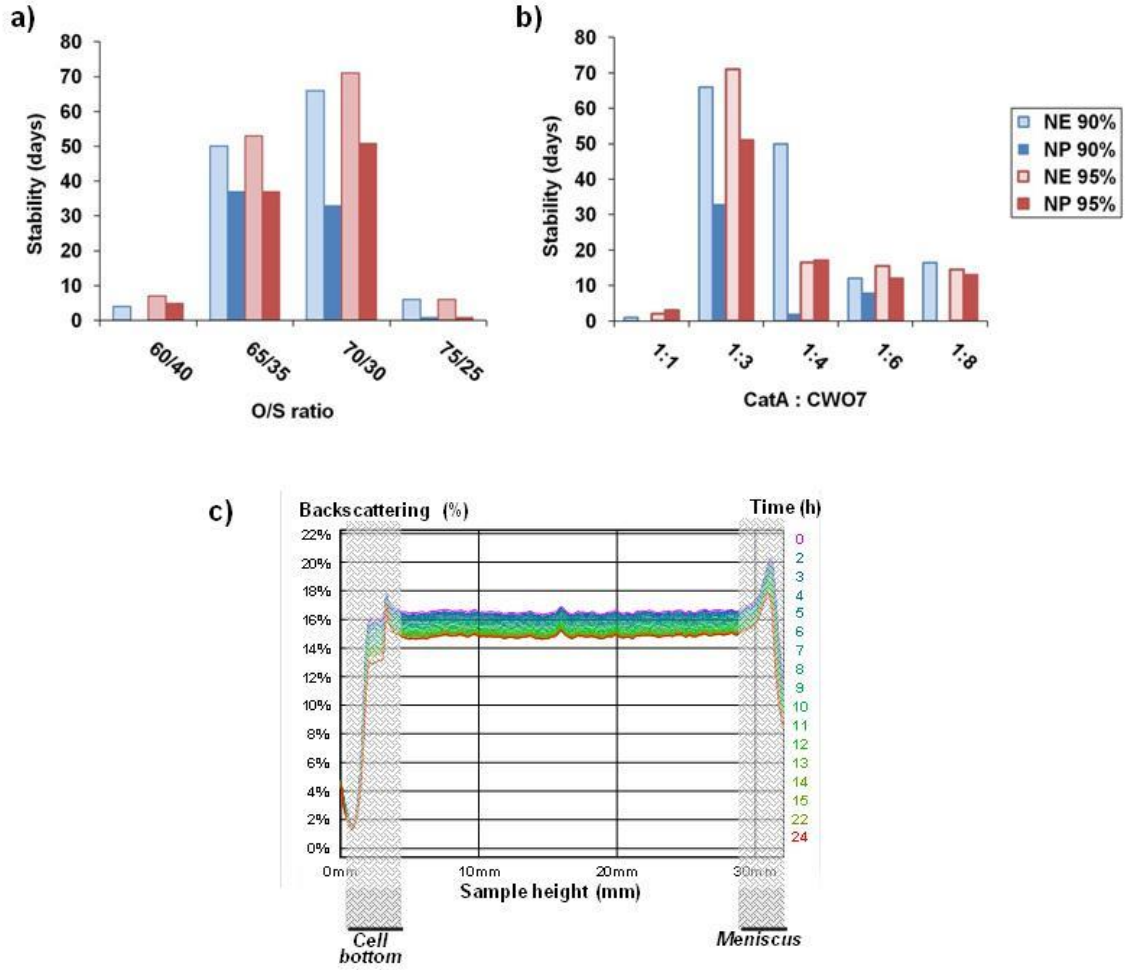

Figure 8: Stability visually assessed as a function of the oil-to-surfactant ratio (O/S) at a constant CatA:CWO7= 1:3 **(a)** and the CatA:CWO7 ratio at a constant O/S=70/30 **(b)** of the nano-emulsions and the nanoparticle dispersions as assessed visually in the Water / [CatA:CWO7] / [6 wt% EC10 in ethyl acetate] system with 90 and 95 wt% water content at 25ºC; and **c)** Backscattering data of the nano-emulsion with an O/S ratio of 70/30, 95 wt% of water content and 6 wt% EC10 with the mixed CatA:CWO7 ratio of 1:3.

4. CONCLUSIONS

O/W nano-emulsions have been formed by the PIC method in the Water / [CatA:CWO7=1:3] / [6% EC10 in ethyl acetate] system in a small region, close to the water vertex in the pseudo-ternary diagram, at O/S ratios between 55/45 and 75/25 and above 88 wt% water at 25ºC. The nano-emulsion domain keeps unchanged when modifying the CatA:CWO7 ratio to 1:1 and decreases when

increasing the EC10 concentration to 10 wt% in the oil component. Nano-emulsions with an O/S ratio of 70/30 form over a broad CatA:CWO7 ratio range, both at 90 and 95 wt% water. The nano-emulsions studied showed droplet sizes below 200 nm and zeta potential values up to about 50 mV. Both, droplet size and zeta potential values of the nano-emulsions vary in a defined trend as a function of their composition, and the nanoparticles obtained from them show sizes and zeta potential values close to those of their template nano-emulsions. The most suitable CatA:CWO7 ratio for nano-emulsion formation is 1:3 and an O/S ratio of 70/30 as at these ratios smallest droplet sizes, high zeta potential values and optimal stability are attained. At a fixed CatA:CWO7 ratio of 1:3, particle size varies in a narrow range of about 20 nm when varying O/S ratios between 60/40 and 70/30, showing a smooth decrease in zeta potential (ranging over about 10 mV), both, at water contents of 90wt% and 95 wt%. However, when varying the CatA:CWO7 ratio at a constant O/S ratio of 70/30, particle size varies following a parabolic trend over a range of about 60 nm, reaching minimal nanoparticle sizes as small as 110 nm at a CatA:CWO7 ratio of 1:3. In contrast, to the effect of the oil-to-surfactant ratio, zeta potential decreases notably with CatA:CWO7, namely over about 30 mV, in the range between CatA:CWO7 of 1:1 and 1:8. Hence, in the system studied, the CatA:CWO7 ratio has the highest influence on both, the particle size and the zeta potential, followed by the O/S ratio and the water content (90 or 95 wt%). This demonstrates that, size and surface charge of the ethylcellulose nanoparticles prepared in this system can be controlled by tuning the composition of the nano-emulsion template. Interestingly, the positive charge of the nanoparticles can be depleted under diluting conditions in a time-dependent manner over a period of days.

5. CONFLICTS OF INTEREST

The authors declare no conflict of interests.

6. ACKNOWLEDGEMENTS

The DLS, zeta potential, viscosity and Turbiscan analyses have been performed at the Nanostructured Liquid Characterization Unit, located at the Institute of Advanced Chemistry of Catalonia (IQAC), belonging to the Spanish National Research Council (CSIC) and affiliated to the NANBIOSIS ICTS of the Biomedical Networking Center (CIBER-BBN). CIBER-BBN is an initiative funded by the VI National R&D&I Plan 2008-2011. Financial support from MINECO (grant CTQ2011-29336-C03-01 and CTQ2017-84998-P) and Generalitat de Catalunya (grant 2017 SGR 1778) is acknowledged. S.L. is grateful to CIBER-BBN for a research scholarship. Colorcon and Bonderalia S.A./Quimivita S.A. are gratefully acknowledged for the gift of ethylcellulose and ricinoleamidopropyltrimonium methosulfate respectively.

7. REFERENCES

Balzus B, Sahle FF, Hönzke St, Gerecke Ch, Schumacher F, Hedtrich S, Kleuser B, Bodmeier R. Formulation and ex vivo evaluation of polymeric nanoparticles for controlled delivery of corticosteroids to the skin and the corneal epithelium. European Journal of Pharmaceutics and Biopharmaceutics 2017; 115: 122–130

Božič M, Elschner Th, Tkaučič D, Bračič M, Hribernik S, Kleinschek KS, Kargl R. Effect of different surface active polysaccharide derivatives on the formation of ethyl cellulose particles by the emulsion solvent evaporation method. Cellulose 2018; 25:6901–6922

Brown W., Dynamic Light Scattering: The Method and Some Applications, Oxford University Press, New York, 1993.

Burgos-Mármol JJ, Solans C, Patti A. effective short-range Coulomb correction to model the aggregation behavior of ionic surfactants. J Chem Phys 2016; 144: 234904

772 Calderó G, García-Celma MJ, Solans C. Formation of polymeric nano-
773 emulsions by a low-energy method and their use for nanoparticle preparation J
774 Colloid Interface Sci 2011; 353: 406–411

775 Calderó G, Montes R, Llinàs M, García-Celma MJ, Porras M, Solans C. Studies
776 on the formation of polymeric nano-emulsions obtained via low-energy
777 emulsification and their use as templates for drug delivery nanoparticle
778 dispersions. Colloids and Surfaces B: Biointerfaces 2016; 145: 922–931

779 Cao M., Wang M, Li L, Qiu H, Yang Z. Effect of Graphene-EC on Ag NW-
780 Based Transparent Film Heaters: Optimizing the Stability and Heat Dispersion
781 of Films. ACS Applied Materials and Interfaces 2018; 10 (1): 1077-1083

782 Chang Y, McLandsborough L, McClements DJ. Fabrication, stability and
783 efficacy of dual-component antimicrobial nanoemulsions: Essential oil (thyme
784 oil) and cationic surfactant (lauric arginate). Food Chemistry 2015; 172: 298–
785 304

786 Crabbe-Mann M, Tsaoulidis D, Parhizkar M, Edirisinghe M. Ethyl cellulose,
787 cellulose acetate and carboxymethyl cellulose microstructures prepared using
788 electrohydrodynamics and green solvents. Cellulose 2018; 25: 1687-1703

789 Davidovich-Pinhas M, Barbut S., Marangoni AG. Physical structure and thermal
790 behavior of ethylcellulose. Cellulose 2014; 21: 3243–3255

791 Davidovich-Pinhas, M., Barbut, S., Marangoni, A.G. The gelation of oil using
792 ethyl cellulose. Carbohydrate Polymers 2015: 17; 869-878.

793 Delgado, AV, González-Caballero F, Hunter RJ, Koopal LK, Lyklema J.
794 Measurement and interpretation of electrokinetic phenomena. J Colloid
795 Interface Sci 2007; 309 (2): 194-224

796 Djerafi R, Masmoudi Y, Crampon C, Meniai A, Badens E. Supercritical anti-
797 solvent precipitation of ethyl cellulose. J. of Supercritical Fluids 2015; 105: 92–
798 98

799 Elek N, Hoffman R, Raviv U, Resh R, Ishaaya I, Magdassi S. Novaluron
800 nanoparticles: Formation and potential use in controlling agricultural insect
801 pests. Colloids and Surfaces A: Physicochemical and Engineering Aspects
802 2010; 372 (1-3): 66-72

803 Eltayeb M, Stride E, Edirisinghe M. Preparation, characterization and release
804 kinetics of ethylcellulose nanoparticles encapsulating ethylvanillin as a model
805 functional component. J Functional Foods 2015; 14: 726–735

806 Generalova AN, Sizova SV, Oleinikov VA, Zubov VP, Artemyev MV, Spernarth
807 L, Kamyshny A, Magdassi S. Highly fluorescent ethyl cellulose nanoparticles
808 containing embedded semiconductor nanocrystals. Colloids Surfaces A:
809 Physicochemical and Engineering Aspects 2009; 342 (1-3): 59-64

810 Giarra S, Zappavigna S, Campani V, Abate M, Cossu AM, Leonetti C, Porru M,
811 Mayol L , Caraglia M, De Rosa G. Chitosan-Based Polyelectrolyte Complexes
812 for Doxorubicin and Zoledronic Acid Combined Therapy to Overcome Multidrug
813 Resistance. Pharmaceutics 2018; 10: 180-192; doi:10.3390/
814 pharmaceutics10040180

815 Gravelle AJ, Marangoni AG. Ethylcellulose Oleogels: Structure, Functionality,
816 and Food Applications. Advances in Food and Nutrition Research 2018; 84: 1-
817 56

818 Gunduz O, Ahmad Z, Stride E, Edirisinghe M. Continuous Generation of Ethyl
819 Cellulose Drug Delivery Nanocarriers from Microbubbles. Pharm Res 2013; 30:
820 225–237

821 Hayden DR, Kibbelaar HVM, Imhof, A, Velikov KP. Size and Optically Tunable
822 Ethyl Cellulose Nanoparticles as Carriers for Organic UV Filters. ChemNanoMat
823 2018; 4: 301 –308

824 He Ch, Hu Y, Yin L, Tang C, Yin Ch. Effects of particle size and surface charge
825 on cellular uptake and biodistribution of polymeric nanoparticles. Biomaterials
826 2010; 31: 3657-3666

827 Heseltine PhL, Ahmed J, Edirisinghe M. Developments in Pressurized Gyration
828 for the Mass Production of Polymeric Fibers. Macromol Mater Eng 2018;
829 303,1800218

830 Heurtault B, Saulnier P, Pech B, Proust JE, Benoit JP. Physico-chemical
831 stability of colloidal lipid particles. Biomaterials 2003; 24: 4283–4300

832 Hiew TN, Tan DLH, Tiang YL, Heng PWS. Understanding the release
833 performance of pellets with hydrophobic inclusions in sustained-release coating.
834 Int J Pharm 2019; 557: 229–237

835 Jiang J, Oberdörster G, Biswas P. Characterization of size, surface charge and
836 agglomeration state of nanoparticle dispersions for toxicological studies. J
837 Nanopart Res 2009; 11: 77-89

838 Kashkouli KI, Torkzadeh-Mahani M, Mosaddegh E. Synthesis and
839 characterization of a novel organosilane-functionalized chitosan nanocarrier as
840 an efficient gene delivery system: Expression of green fluorescent protein. Int J
841 Biological Macromolecules 2019; 125: 143-148

842 Kim TH, Hong IT, Oh JM. Size- and surface charge-controlled layered double
843 hydroxides for efficient algal flocculation. Environ Sci Nano, 2018; 5: 183-190

844 Kolliphor Grades-Emulsifier for topical pharmaceutical applications. Technical
845 information. 03-12061e-01 January 2014. WF-N0.125032

846 Leitner S, Solans C, García-Celma MJ, Calderó G. Low-energy nano-
847 emulsification approach as a simple strategy to prepare positively charged
848 ethylcellulose nanoparticles. Carbohydrate Polymers 2019; 205: 117–124

849 Lin MH, Hung ChF, Aljuffali IA, Sung CT, Huang ChT, Fang JY. Cationic
850 amphiphile in phospholipid bilayer or oil–water interface of nanocarriers affects
851 planktonic and biofilm bacteria killing. Nanomedicine: Nanotechnology, Biology,
852 and Medicine 2017; 13: 353–361

853 Mimi N, Belkacemi H, Sadoun T, Sapin A, Maincent P. How the composition
854 and manufacturing parameters affect insulin release from polymeric
855 nanoparticles. Journal of Drug Delivery Science and Technology 2015; 30: 458-
856 466

857 Monpara J, Velga D, Verma T, Gupta S, Vavia P. Cationic cholesterol derivative
858 efficiently delivers the genes: in silico and in vitro studies. Drug Delivery and
859 Translational Research 2019; 9: 106-122

860 Qi L, Xu Z, Jiang X, Hu C, Zou X. Preparation and antibacterial activity of
861 chitosan nanoparticles. Carbohydrate Research 2004; 339: 2693–2700

862 Obst K, Yealland G, Balzus B, Miceli E, Dimde M, Weise Ch, Eravci M,
863 Bodmeier R, Haag R, Calderón M, Charbaji N, Hedtrich S. Protein Corona
864 Formation on Colloidal Polymeric Nanoparticles and Polymeric Nanogels:
865 Impact on Cellular Uptake, Toxicity, Immunogenicity, and Drug Release
866 Properties. Biomacromolecules 2017, 18, 1762−1771

867 Pecora R. Dynamic light scattering measurement of nanometer particles in
868 liquids. J Nanopart Res 2000; 2: 123–131 http://dx.doi.org/10.1023/
869 A:1010067107182.

870 Pires RM, Costa HF, Ferreira AGM, Fonseca MA. Viscosity and Density of
871 Water + Ethyl Acetate + Ethanol Mixtures at 298.15 and 318.15 K and
872 Atmospheric Pressure. J Chem Eng Data 2007; 52: 1240-1245

873 Rodríguez C, Acharya DP, Maestro A, Hattori K, Aramaki K, Kunieda H. Effect
874 of nonionic head group size on the formation of worm-like micelles in mixed
875 nonionic/cationic surfactant aqueous systems. J Chem Eng Japan 2004; 37 (5):
876 622-629

877 Sadurní N, Solans C, Azemar N, García-Celma MJ. Studies on the formation of
878 O/W nano-emulsions, by low-energy emulsification methods, suitable for
879 pharmaceutical applications. Eur. J. Pharm. Sci. 2005; 26: 438

880 Smith MC, Crist RM, Clogston JD, McNeil SE. Zeta potential: a case study of
881 cationic, anionic, and neutral liposomes. Anal Bioanal Chem 2017; 409:5779–
882 5787

883 Spernarth L, Magdassi S. Preparation of ethyl cellulose nanoparticles from
884 nano-emulsion obtained by inversion at constant temperature. Micro and Nano
885 Letters 2007; 2 (4): 90-95

886 Vílchez-Maldonado S, Calderó G, Esquena J. Molina R. UV protective textiles
887 by the deposition of functional ethylcellulose nanoparticles. Cellulose 2014;
888 21:2133–2145

889 Wanga D, Tana J, Kanga H, Ma L, Jin X, Liu R, Huang Y. Synthesis, self-
890 assembly and drug release behaviors of pH-responsive copolymers ethyl
891 cellulose-graft-PDEAEMA through ATRP. Carbohydrate Polymers 2011; 84:
892 195–202

Zuo X, Wu J, Ma X, Deng X, Cai J, Chen Q, Liu J, Nan J. A poly(vinylidene fluoride)/ethyl cellulose and amino-functionalized nano-SiO_2 composite coated separator for 5 V high-voltage lithium-ion batteries with enhanced performance. J Power Sources 2018; 407 (15): 44-52

Supplementary Information 1

The refractive indexes and the viscosities required for the DLS measurements (Section 2.2.5.) were determined experimentally as explained next. The continuous phases of representative nano-emulsions and nanoparticle dispersions were obtained by centrifugal phase separation at 25ºC. Water saturated with ethyl acetate was prepared by mixing ethyl acetate with water at a ratio of ethyl acetate:water = 20:80 in a stoppered flask, and then allowing the mixture to phase separate in a separating funnel thermostated at a constant temperature of 25ºC.

The refractive indexes of the continuous phases as measured at least in triplicate by means of an Abbe refractometer (Atago 3T) at 25ºC were 1.3358 ± 0.0002 for the nano-emulsion and 1.3334 ± 0 for the nanoparticle dispersion.

The viscosity of the samples was measured in duplicate on a AR-G2 Rheometer (TA Instruments Ltd) using concentric cylinders, at a shear rate range between 1 and 200 s^{-1} and a temperature of 25ºC. The viscosity of the continuous phase of the nano-emulsion was 1.005 ± 0.026 cP and that of the nanoparticle dispersion 0.937 ± 0.006 cP. The higher viscosity of the continuous phase of the nano-emulsion as compared to that of the nanoparticle dispersion is attributed to the presence of ethyl acetate. This solvent is partially soluble in water (around 7.7 wt% at 25ºC (Calderó et al. 2011 and 2016)) and has been reported to undergo intermolecular dipolar interactions with the water molecules producing a significant viscosity increase in a certain concentration range in water, as also observed in our system (Pires et al. 2007).It is worth mentioning that the refractive index and viscosity of water saturated with ethyl acetate are 1.3490 ± 0 and 1.073 ± 0.093 cP respectively, while the reported values for pure ethyl acetate are 1.3720 (refractive index) and 0.426 cP respectively. These data suggest that the continuous phase of the nano-emulsion is not saturated with ethyl acetate. In addition, the viscosity of the continuous phase of the nanoparticle dispersion is higher than that of pure water at 25ºC (0.879 ± 0.008 cP). This is attributed to the presence of the surfactants in this phase. Some surfactant mixture excess might also be present in the continuous phase of the nano-emulsions.

Supplementary Information 2

Zeta potential values of the nanoparticle dispersion as a function of time, measured during dialysis of the nanoparticle dispersion obtained from a nano-emulsion of the Water / [CatA:CWO7 = 1:3] / [6 wt% EC10 in ethyl acetate] system with an O/S ratio of 70/30 and 95 wt% water content.

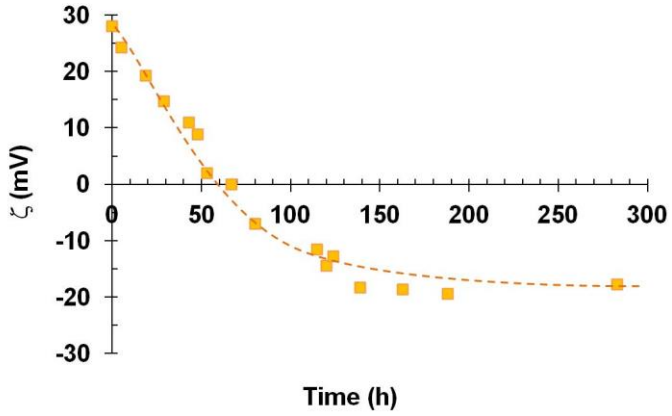

Supplementary Information 3

Theoretical stability assessment of nano-emulsions of the Water / [CatA:CWO7] / [6 wt% EC10 in ethyl acetate] system with an O/S ratio of 70/30 and 90 and 95 wt% water, calculated from Stokes'law. Droplet migration velocity is given in absolute values and nm/s.

CatA:CWO7 ratio	Migration rate (nm/s)	
	90 wt%	95 wt%
1:1	1.4	1.8
1:3	0.8	0.8
1:4	0.9	1.0
1:6	1.1	1.2
1:8	1.7	1.6